Second-order topological insulator in a coinless discrete-time quantum walk

Ya Meng,[1] Gang Chen,[1,2,3,*] and Suotang Jia[1,2]

[1]*State Key Laboratory of Quantum Optics and Quantum Optics Devices, Institute of Laser Spectroscopy, Shanxi University, Taiyuan 030006, China*

[2]*Collaborative Innovation Center of Extreme Optics, Shanxi University, Taiyuan, Shanxi 030006, China*

[3]*Collaborative Innovation Center of Light Manipulations and Applications, Shandong Normal University, Jinan 250358, China*

(Received 17 March 2020; accepted 12 June 2020; published 7 July 2020)

Higher-order topological insulators not only exhibit the exotic bulk-boundary correspondence principle but also have an important application in quantum computing. However, it seems they have not been achieved in the discrete-time quantum walk. In this paper we construct a two-dimensional coinless discrete-time quantum walk to simulate the second-order topological insulator with zero-dimensional corner states. We show that both of the corner and edge states can be observed through the probability distribution of the walker after a multistep coinless discrete-time quantum walk. Finally, we propose a possible experimental implementation to realize this coinless discrete-time quantum walk in a three-dimensional integrated photonic circuit and verify the robustness of the corner states against the small disorder. Our work offers an alternative route to explore exotic higher-order topological matters using discrete-time quantum walks.

DOI: 10.1103/PhysRevA.102.012203

I. INTRODUCTION

The quantum walk, which describes the propagation of quantum particles on a lattice [1–4], is a quantum version of the classical random walk. Due to its simplicity and high controllability, the quantum walk has become a powerful tool for universal quantum computing [5,6] and quantum simulation [7–10]. Inspired by an original theoretical paper of Kitagawa *et al.* [11], the discrete-time quantum walk (DTQW) has become an outstanding platform for simulating various topological phenomena [12–20]. In particular, the topological edge states and winding numbers have been detected by both unitary [21–26] and nonunitary [27–31] one-dimensional DTQWs. For the two-dimensional case, the one-dimensional edge states have been observed without [32,33] and with [34] the synthetic gauge field. Very recently, the Chern number has been successfully probed by an anomalous displacement [35]. Note that the above topological simulations are achieved in the coined DTQW with the intrinsic coin states, the one-step evolution operator of which contains both the translation and coin operators. Without introducing the coin states, the coinless DTQW emerges [36–42]. In such cases, the corresponding one-step evolution operator has the translation operator acting only in the site basis. This means that the coinless DTQW possesses a smaller Hilbert space. Recently, the walk dynamics on different topologies have been revealed in the two-dimensional coinless DTQW [43].

However, current research on topological features of both the coined and coinless DTQWs focus only on the simulation of the first-order topological insulator, which supports topological protected states in the $(d-1)$ -dimensional boundaries for a d-dimension system. Recently, higher-order topological insulators, which have lower-dimensional gapless boundary states, have attracted much attention in both theory [44–48] and experiment [49–56]. Physically, these higher-order topological insulators exhibit an exotic bulk-boundary correspondence principle that an nth-order topological insulator supports gapless $(d-n)$-dimensional boundary states. Moreover, these gapless boundary states can support nontrivial fractional quasiparticles (such as parafermion or Ising anyon, etc.), providing a new architecture for quantum information processing and quantum computing [57,58].

In this paper we introduce the two-dimensional coinless DTQW to simulate a second-order topological insulator which hosts zero-dimensional corner states and one-dimensional edge states. We show that both the corner and edge states can be observed through the probability distribution of the walker after a multistep coinless DTQW. Finally, we propose a possible experimental implementation in three-dimensional integrated photonic circuits and verify the robustness of the corner states against small disorder. Since the coupling and phase between each of the two lattice sites at each step of the coinless DTQW can be adjusted independently, our proposal can be extended directly to realize other exotic higher-order topological insulators, such as the non-Hermitian [59–64] and Floquet higher-order topological insulators [65–69], which have not been observed in experiments. Our work offers an alternative route to explore exotic topological matters using DTQWs.

This paper is organized as follows. In Sec. II we introduce a two-dimensional coinless DTQW. In Sec. III we demonstrate the existence of the zero-dimensional corner states and the one-dimensional edge states through calculating the spectra and the topological invariant. In Sec. IV we show that the corner and edge states can be observed experimentally through the probability distributions of the walker after a multistep coinless DTQW. In Sec. V we propose a possible

*chengang971@163.com

experimental implementation in a three-dimensional integrated photonic circuit. In Sec. VI we verify the robustness of the corner states against the small disorder. Finally, we give the summarization in Sec. VII.

II. A TWO-DIMENSIONAL COINLESS DTQW

We begin to introduce a two-dimensional Su-Schrieffer-Heeger model with π flux per plaquette, which is governed by the Hamiltonian

$$H=\sum_{x,y}(t_x a^{\dagger}_{x+1,y}a_{x,y}+t_y e^{ix\pi}a^{\dagger}_{x,y+1}a_{x,y})+\text{H.c.}, \tag{1}$$

where $a^{\dagger}_{x,y}$ ($a_{x,y}$) is the creation (annihilation) operator of a spinless particle at the site (x,y), $t_{x(y)}=t+(-1)^{x(y)}\delta t$ are the two types of hopping amplitudes in the x (y) direction, respectively, and can be defined as $J_1=t-\delta t$, $J_2=t+\delta t$, and H.c. is the Hermitian conjugate. The Hamiltonian (1) can host the topologically protected corner states [44,45]. In the following we construct a two-dimensional coinless DTQW to simulate the second-order topological insulator based on this Hamiltonian.

We first divide it into four parts,

$$H=H_{2y}+H_{1y}+H_{2x}+H_{1x}, \tag{2}$$

where H_{1x} (H_{2x}) and H_{1y} (H_{2y}) are the intracellular (intercellular) hoppings along the x and y directions, respectively. We then construct the one-step operator of a coinless DTQW as

$$\begin{aligned}U_{\text{step}}&=e^{-i\frac{\pi}{4}\frac{H_{2y}\Delta T}{\hbar}}e^{-i\frac{\pi}{4}\frac{H_{1y}\Delta T}{\hbar}}e^{-i\frac{\pi}{4}\frac{H_{2x}\Delta T}{\hbar}}e^{-i\frac{\pi}{4}\frac{H_{1x}\Delta T}{\hbar}}\\&=U_4U_3U_2U_1.\end{aligned} \tag{3}$$

For simplicity, we use the units $\Delta T=\hbar=1$ hereafter. For the Hamiltonian (1), these four substep operators are chosen as

$$U_1=\sum_{x=0}^{M/2-1}V_{2x+1}\otimes\mathcal{I}_y, \tag{4}$$

$$U_2=(|1\rangle_x\langle 1|+|M\rangle_x\langle M|)\otimes\mathcal{I}_y+\sum_{x=1}^{M/2-1}V_{2x}\otimes\mathcal{I}_y, \tag{5}$$

$$U_3=\sum_{x=1}^{M}\sum_{y=0}^{M/2-1}|x\rangle\langle x|\otimes V_{2y+1}, \tag{6}$$

$$\begin{aligned}U_4=&\mathcal{I}_x\otimes(|1\rangle_y\langle 1|+|M\rangle_y\langle M|)\\&+\sum_{x=1}^{M}\sum_{y=1}^{M/2-1}|x\rangle\langle x|\otimes V_{2y},\end{aligned} \tag{7}$$

where the translation operators in the x and y directions are defined as

$$\begin{aligned}V_x=&\cos\left(\frac{\pi}{4}r\right)[|x\rangle\langle x|+|x+1\rangle\langle x+1|]\\&-i\sin\left(\frac{\pi}{4}r\right)[|x+1\rangle\langle x|+|x\rangle\langle x+1|],\end{aligned} \tag{8}$$

$$\begin{aligned}V_y=&\cos\left(\frac{\pi}{4}r\right)[|y\rangle\langle y|+|y+1\rangle\langle y+1|]\\&-i\sin\left(\frac{\pi}{4}r\right)[e^{ix\pi}|y+1\rangle\langle y|+e^{-ix\pi}|y\rangle\langle y+1|].\end{aligned} \tag{9}$$

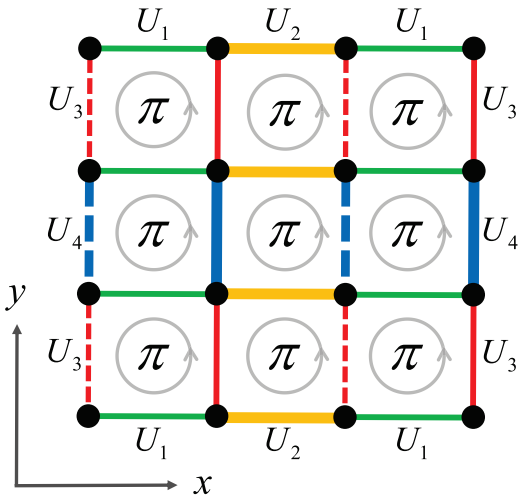

FIG. 1. The proposed implementation of a coinless DTQW in a two-dimensional lattice. The links of the lattice are marked with different colors, degrees of thickness, and line types, respectively. The different colors represent four substep operators U_i in Eqs. (4)–(7), respectively. The links with the different thicknesses represent two types of hopping amplitudes, J_1 and J_2, respectively. The dashed lines in the y direction indicate the required $\pm\pi$ phases of the hopping amplitudes, which can induce a π flux when a walker goes through an elementary cell anticlockwise.

We have $r=J_1$ ($r=J_2$) for the substep operators U_1 and U_3 (U_2 and U_4). This coinless DTQW is implemented in the Hilbert space $|x\rangle\otimes|y\rangle$, with $x\in\{1,M\}$ and $y\in\{1,M\}$ (M is even). The operator $\mathcal{I}_{x(y)}$ denotes a $M\times M$ identity matrix in the sub-Hilbert space $|x\rangle$ ($|y\rangle$). These four substep operators in Eqs. (4)–(7) do not commute with each other and can be adjusted independently. It should be emphasized that in order to generate the π flux per plaquette, here we have added key phase factors of the translation operator V_y. By applying the one-step operator in Eq. (3) many times, a multistep coinless DTQW can be realized, as shown schematically in Fig. 1, and the topologically protected corner states can be explored, as will be shown.

III. SPECTRA AND TOPOLOGICAL INVARIANT

In order to illustrate the topological features of this coinless DTQW, here we discuss the quasienergy spectrum and the topological invariant. In Fig. 2(a), we plot the quasienergy spectrum of the effective Hamiltonian, $H_{\text{eff}}=i\ln U_{\text{step}}$, under the open boundary condition. This figure shows clearly that the gapless zero-energy and gapped nonzero-energy states can occur. Moreover, the gapless zero-energy states are four-degenerate and separated from the bulk states by a large energy gap, while these four-degenerate gapped nonzero-energy states are separated from the bulk states only with a tiny gap, as shown in Fig. 2(b). When we increase the parameter J_1, this tiny band gap disappears quickly. In Fig. 2(c) we plot the collective distributions of these four-degenerate zero- and nonzero-energy states, which are indeed localized at the four corners and edges of the lattice, respectively.

The appearance of the zero-dimensional corner states can be attributed to the second-order bulk topology, which is

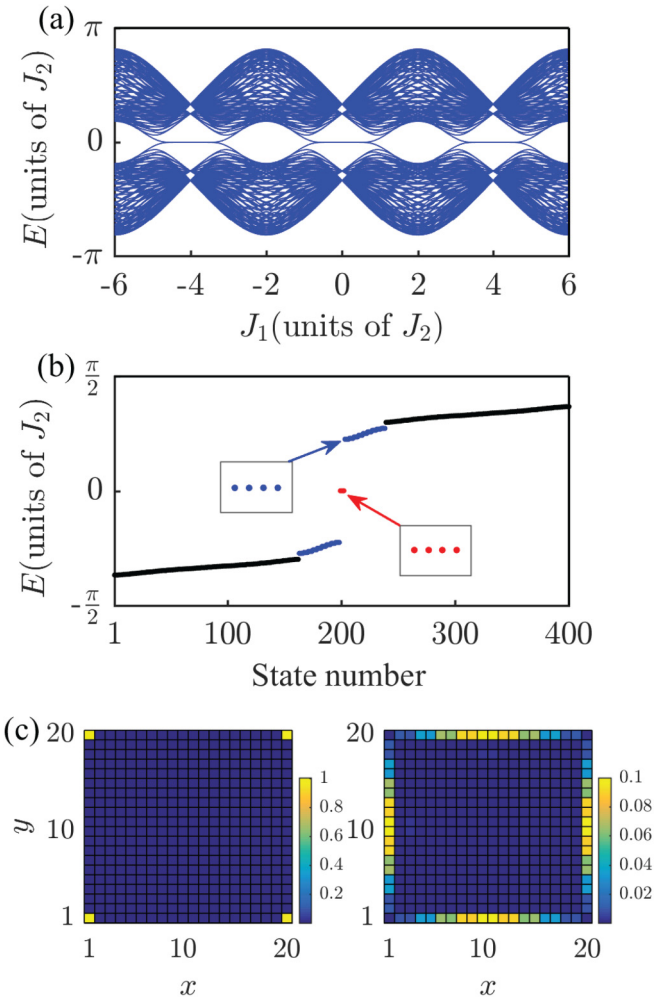

FIG. 2. (a) The quasienergy spectrum of the effective Hamiltonian, $H_{\text{eff}} = i \ln U_{\text{step}}$, as a function of the parameter J_1. (b) The quasienergy spectrum with $J_1/J_2 = 0.1$. There are four-degenerate zero- and nonzero-energy states, respectively denoted by the red and blue points. (c) Left: Collective distribution of the four-degenerate zero-energy corner-localized states. Right: Collective distribution of the four-degenerate nonzero-energy edge-localized states with state numbers {203, 204, 205, 206}. Here the lattice size is chosen as 20×20.

described by introducing the Wannier bands and the nested Wilson loops [44,45]. Generally speaking, the complete characterization of the second-order topology for a Floquet system gives a pair of $\mathbb{Z}_2$ invariant, which can predict the appearance of zero- and π-corner states [65–69]. For our model, only one $\mathbb{Z}_2$ invariant is enough with the absence of the π-corner states.

To construct the topological invariant, we consider the eigenstates of the one-step operator in momentum representation,

$$U_{\text{step}}(\mathbf{k})|E_{\mathbf{k}}\rangle = e^{-iE_{\mathbf{k}}}|E_{\mathbf{k}}\rangle, \tag{10}$$

where two gapped bands with the quasienergy $\pm E_{\mathbf{k}}$ are doubly degenerate, respectively, and the eigenstates can be denoted as $|+E^1_{\mathbf{k}}\rangle$ and $|+E^2_{\mathbf{k}}\rangle$ ($|-E^1_{\mathbf{k}}\rangle$ and $|-E^2_{\mathbf{k}}\rangle$) for upper (lower) bands. When the lower two bands are filled, the Wilson loop operator in the x direction is defined as

$$\mathcal{W}_{x,\mathbf{k}} = F_{x,\mathbf{k}+(N_x-1)\Delta k_x \mathbf{e}_x} \cdots F_{x,\mathbf{k}+\Delta k_x \mathbf{e}_x} F_{x,\mathbf{k}}, \tag{11}$$

where $F_{x,\mathbf{k}}$ is a 2×2 matrix with element $[F_{x,\mathbf{k}}]^{mn} = \langle -E^m_{\mathbf{k}+\Delta k_x \mathbf{e}_x}| - E^n_{\mathbf{k}}\rangle (m, n = 1, 2)$, $\mathbf{e}_x$ is the unit vector in the x direction, and $\Delta k_x = 2\pi/N_x$. The two-dimensional Brillouin zone is discretized by using the interval $(2\pi/N_x, 2\pi/N_y)$ such that there are $(N_x + 1)(N_y + 1)$ k points in total. With the periodic boundary condition, $|-E^n_{\mathbf{k}}\rangle = |-E^n_{\mathbf{k}+2\pi \mathbf{e}_x}\rangle$, we diagonalize Eq. (11) as

$$\mathcal{W}_{x,\mathbf{k}}\big|\mathrm{v}^j_{x,\mathbf{k}}\big\rangle = e^{i2\pi \mathrm{v}^j_x(k_y)}\big|\mathrm{v}^j_{x,\mathbf{k}}\big\rangle, \tag{12}$$

where $j = \pm$ denotes two Wannier bands. These Wannier bands carry their own topological invariants, which can be evaluated by calculating the nested Wilson loops.

We first construct the Wannier states as

$$|w^{\pm}_{x,\mathbf{k}}\rangle = \sum_{n=1,2} [\mathrm{v}^{\pm}_{x,\mathbf{k}}]^n \big| - E^n_{\mathbf{k}}\big\rangle, \tag{13}$$

where $[\mathrm{v}^{\pm}_{x,\mathbf{k}}]^n$ denotes the nth element of the two-component spinor $|\mathrm{v}^{\pm}_{x,\mathbf{k}}\rangle$. Then, with the periodic boundary condition, $|w^{\pm}_{x,\mathbf{k}}\rangle = |w^{\pm}_{x,\mathbf{k}+2\pi \mathbf{e}_y}\rangle$, the nested Wilson loops along k_y in the Wannier bands $\mathrm{v}^{\pm}_x$ are

$$\tilde{\mathcal{W}}_{y,\mathbf{k}} = F^{\pm}_{y,\mathbf{k}+(N_y-1)\Delta k_y \mathbf{e}_y} \cdots F^{\pm}_{y,\mathbf{k}+\Delta k_y \mathbf{e}_y} F^{\pm}_{y,\mathbf{k}}, \tag{14}$$

where $F^{\pm}_{y,\mathbf{k}} = \langle w^{\pm}_{x,\mathbf{k}+\Delta k_y \mathbf{e}_y}|w^{\pm}_{x,\mathbf{k}}\rangle$, $\mathbf{e}_y$ is the unit vector in the y direction, and $\Delta k_y = 2\pi/N_y$. Through Eq. (14) we obtain the nested polarization as

$$p_y^{\mathrm{v}^{\pm}_x} = -\frac{i}{2\pi}\frac{1}{N_x}\sum_{k_x} \log[\tilde{\mathcal{W}}^{\pm}_{y,\mathbf{k}}]. \tag{15}$$

Similarly, we can also obtain the nested polarization $p_x^{\mathrm{v}^{\pm}_y}$ from the nest Wilson loops in the y direction. Finally, the topological quadrupole phase is characterized by a $\mathbb{Z}_2$ invariant [44],

$$\nu = 4 p_y^{\mathrm{v}^{\pm}_x} p_x^{\mathrm{v}^{\pm}_y}. \tag{16}$$

By choosing $N_x = N_y = 50$, we numerically calculate the topological invariant ν by using the above procedure. As shown in Fig. 3, we find that the topological invariant ν is

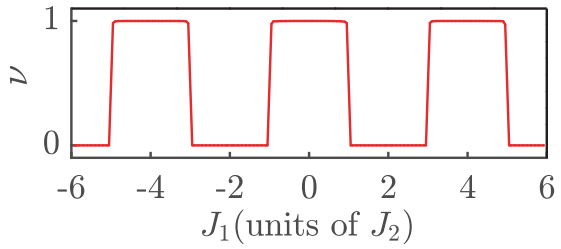

FIG. 3. Numerical plot of the topological invariant ν by the nested Wilson loops. The two-dimensional Brillouin zone is discretized by using 51 k points in each direction.

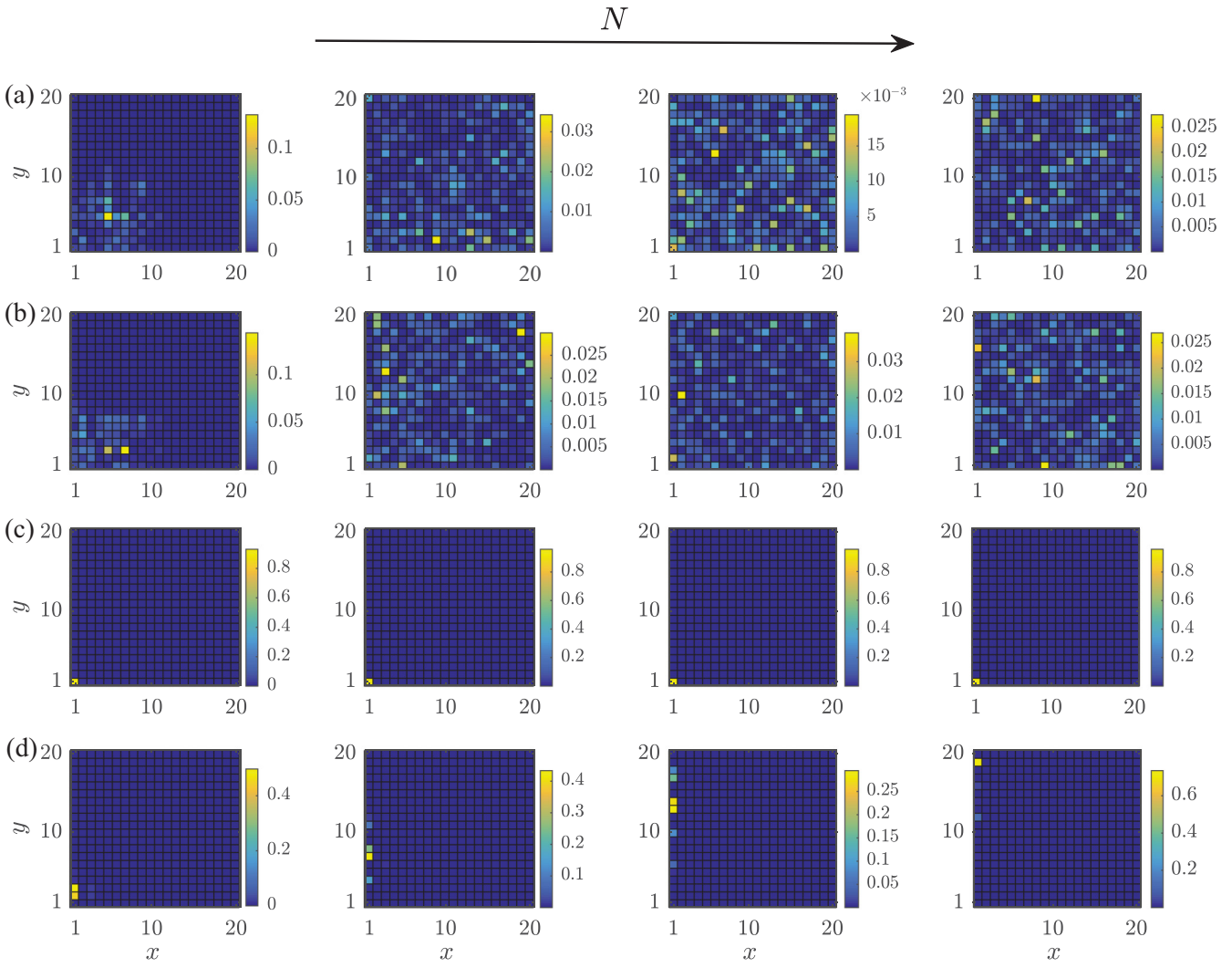

FIG. 4. The probability distributions of the coinless DTQW on a 20 × 20 lattice for steps $N = 5, 50, 100, 150$. The walker is initialized at one corner $(x, y) = (1, 1)$ (a, c) or edge $(x, y) = (1, 2)$ (b, d) of the lattice. In (a, b), the parameter $J_1/J_2 = 1.5$, which corresponds to a trivial phase. In (c, d), the parameter $J_1/J_2 = 0.1$, which corresponds to a quadrupole topological phase.

quantized to be 0 or 1, which corresponds to the trivial or topological phases, respectively.

IV. OBSERVATION OF THE CORNER AND EDGE STATES

In this section we mainly show that the corner and edge states can be observed experimentally through the probability distribution of the walker after a multistep coinless DTQW. It is well known that the probability distributions of the multistep DTQW exhibit the ballistic behaviors [1–4], which are entirely different from the diffusive behaviors of the classic version. Utilizing this feature, we can demonstrate the existence of the corner and edge states through the local behavior of the probability distribution of the walker.

In the first case we tune the parameter $J_1/J_2 = 1.5$, which corresponds to a trivial phase. We initialize the walker at one corner of the lattice $(x, y) = (1, 1)$ or one edge of the lattice with $(x, y) = (1, 2)$. Since the system does not support any localized states, the probability of the walker spreads ballistically into the bulk with increasing the step of the coinless DTQW; see Figs. 4(a) and 4(b). Then we tune the parameter to $J_1/J_2 = 0.1$, which corresponds to a quadrupole topological phase supporting the localized corner and edge states; see Fig. 2(c). In such a case, when this initial state is prepared at one corner of the lattice $(x, y) = (1, 1)$, since it has a large overlap with the corner state, the most part of the walker's wave packet remains localized near $(x, y) = (1, 1)$ as increasing the step of the coinless DTQW; see Fig. 4(c). In Fig. 4(d) we initialize the walker at one edge of the lattice with $(x, y) = (1, 2)$. Similarly, this initial state has a large overlap with the edge states, and we can also observe a large nonvanishing localization at one edge of the lattice. Since the edge states have a vanishing distribution at the corners of the lattice [see Fig. 2(c)], the walker only localizes at one edge of the lattice. It should be noticed that in Fig. 4, we only show the numerical results when the walker is initialed at the bottom-left corner and left edge of the lattice. The results for the other three corners or edges of the lattice are similar and thus are not shown here.

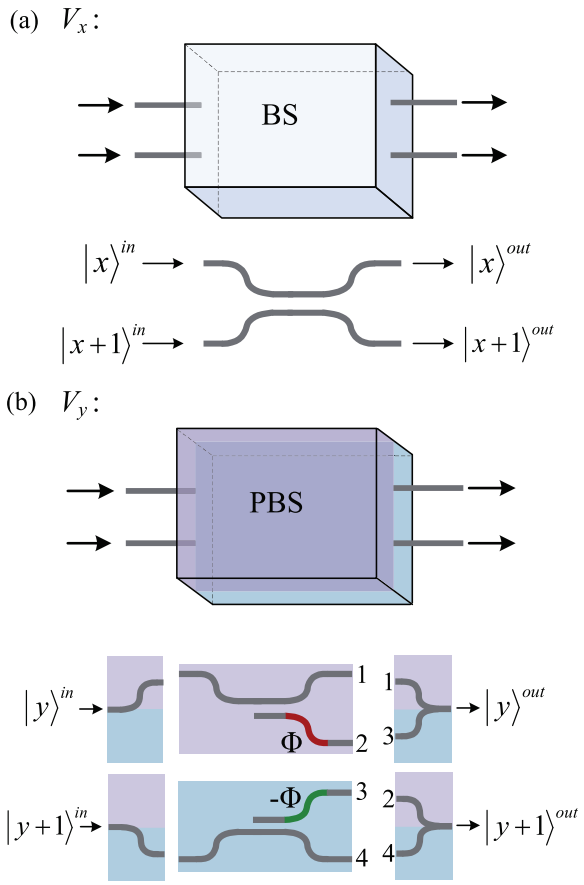

FIG. 5. Scheme of waveguide structure for realizing the translation operators V_x and V_y. (a) A single-layer waveguide structure for realizing a beam splitter (BS). (b) A double-layer waveguide structure for realizing a phase-shifted beam splitter (PBS).

V. POSSIBLE EXPERIMENTAL IMPLEMENTATION

In this section we propose a possible scheme to realize this coinless DTQW in Eq. (3) in a three-dimensional integrated photonic circuit [70], where a single photon acts as a walker and a single waveguide can indicate a two-dimensional lattice site in the x and y directions. The waveguides are extended in the z direction, corresponding to the time dimension of the coinless DTQW. The key to realize this coinless DTQW in experiments is how to achieve the specific translation operators V_x and V_y in Eqs. (8) and (9), which correspond to a beam-splitter matrix and a phased-shifted beam-splitter matrix, respectively. Fortunately, we can realize these translation operators in an integrated photonic circuit with the directional coupler geometry [71], where two waveguides are brought close together for a certain interaction length and coupled by an evanescent field. In the following we will show how to implement the translation operators V_x and V_y with the single- and double-layer waveguide structures, respectively.

The translation operator V_x can be realized by a directional coupler; see Fig. 5(a). The standard coupled-mode theory [72] gives a transfer matrix as

$$T_1(z) = \begin{pmatrix} \cos(Kz) & -i\sin(Kz) \\ -i\sin(Kz) & \cos(Kz) \end{pmatrix}, \tag{17}$$

which can be used to realize Eq. (8). According to Eq. (17), the parameter in V_x can be adjusted through altering the coupling coefficient K and the interaction length z.

Due to the current technology of the full phase-shift controllability between two waveguides [73,74], we can introduce an arbitrary phase in the first (or second) row of $T_1(z)$. However, the phases required in V_y are at the off-diagonal elements of the matrix, which indicates that we cannot realize the translation operator V_y directly by a single directional coupler. Thus we design a double-layer waveguide structure to overcome this limitation. As shown in Fig. 5(b), if a single photon pulse is input from the port labeled by $|y\rangle^{\text{in}}$ (or $|y+1\rangle^{\text{in}}$), it will go through the upper (or lower) layer waveguide structure and obtain a phase Φ (or $-\Phi$). According to the coupled-mode theory, the total transfer matrix governed by this double-layer waveguide structure is

$$T_2(z) = \begin{pmatrix} \cos(Kz) & -i\sin(Kz)e^{i\Phi} \\ -i\sin(Kz)e^{-i\Phi} & \cos(Kz) \end{pmatrix}, \tag{18}$$

which is exactly the phased-shifted beam-splitter matrix in Eq. (9). Thus the experimental implementation of U_{step} is possible with the current technology of the three-dimensional waveguide architecture [75–78]. The phase Φ can be chosen arbitrarily and is here taken as $\Phi = m\pi$, where m is an integer. When m is even, the transfer matrix $T_2(z)$ reduces to $T_1(z)$. That is, a single-layer waveguide structure is enough for this case.

VI. ROBUSTNESS OF CORNER STATES AGAINST SMALL DISORDER

In real experiments the noise usually exists. In the integrated photonic circuits considered above, the noise can be the static or dynamic disorder [73]. To verify the robustness of the corner states in our system, we add the static or dynamic disorder into the evolution processing. The one-step operator for the disorder is introduced as

$$U_{\text{total}} = U_{\text{step}} \times U_{\text{dis}}, \tag{19}$$

with

$$U_{\text{dis}} = \sum_{x,y} e^{i\delta_{x,y}} |x, y\rangle\langle x, y|. \tag{20}$$

Here $\delta_{x,y}$ is chosen randomly from the interval $[-W/2, W/2]$, where W is the disorder strength. For the static disorder, the operator in Eq. (20) is unchanged during the whole evolution processing of a multistep coinless DTQW, while it changes with the steps for the dynamic disorder.

To analyze the robustness of the corner states, we numerically calculate the quasienergy spectrum of the effective Hamiltonian, $H_{\text{eff}} = i \ln U_{\text{total}}$, as a function of the disorder strength. The results are shown in Fig. 6 for 20 independent realizations of disorder. When the disorder strength is small, the corner states are not degenerate but still separated from the edge and bulk states by a wide band gap. This wide band gap indicates that the system is protected by the nontrivial topology with the existence of the robust corner states [50,53,54]. However, when we increase the disorder strength, the band

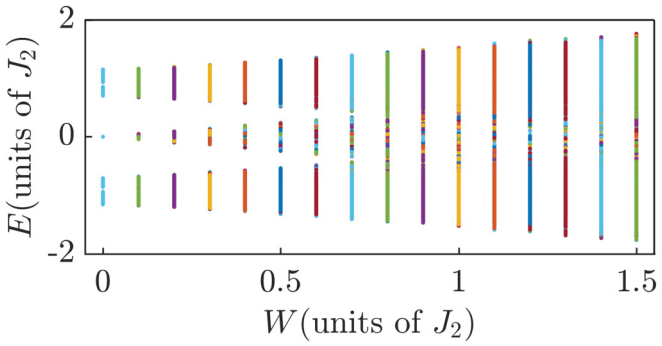

FIG. 6. The quasienergy spectrum of the effective Hamiltonian, $H_{\text{eff}} = i \ln U_{\text{total}}$, as a function of the disorder strength W. The lattice size is chosen as 20×20, and the parameter $J_1/J_2 = 0.1$.

gap will close. The absence of the band gap implies that the nontrivial topology of the system has been destroyed.

Under the small disorder, the robust corner states and the edge states can also be observed experimentally through the probability distributions of the walker. In Fig. 7 we show the probability distributions of the multistep coinless DTQWs with disorder strength $W/J_2 = 0.25$ when the walkers are initialized at the corner and edge of the lattice, respectively. It is clear to see that the walkers always have stable large localizations at the corner and edge, which strongly verifies the existence of the corner and edge states. To show the influence of the disorder strength on the localizations at the corner and edge more clearly, in Fig. 8 we plot the probabilities P_c at the corner $(x, y) = (1, 1)$ and P_e at the left edge of the lattice vs step N with different disorder strengths. When the disorder strength is chosen as $W/J_2 = 0.25$ [see Figs. 8(a) and 8(c)], we can see really large localizations at the corner and edge of the lattice during the whole evolution processing of the coinless DTQWs with the static and dynamic disorders, the results of which are consistent with the probability distributions of the walker shown in Fig. 7. When we increase the disorder strength as $W/J_2 = 0.5$, the probabilities P_c and P_e are still large but with slight decreases [see Figs. 8(b) and 8(d)]. Furthermore, in Fig. 9 we show the probabilities P_c at the corner $(x, y) = (1, 1)$ and P_e at the left edge of the lattice vs the disorder strength. Generally, the stable large localizations at the corner and edge can be observed when

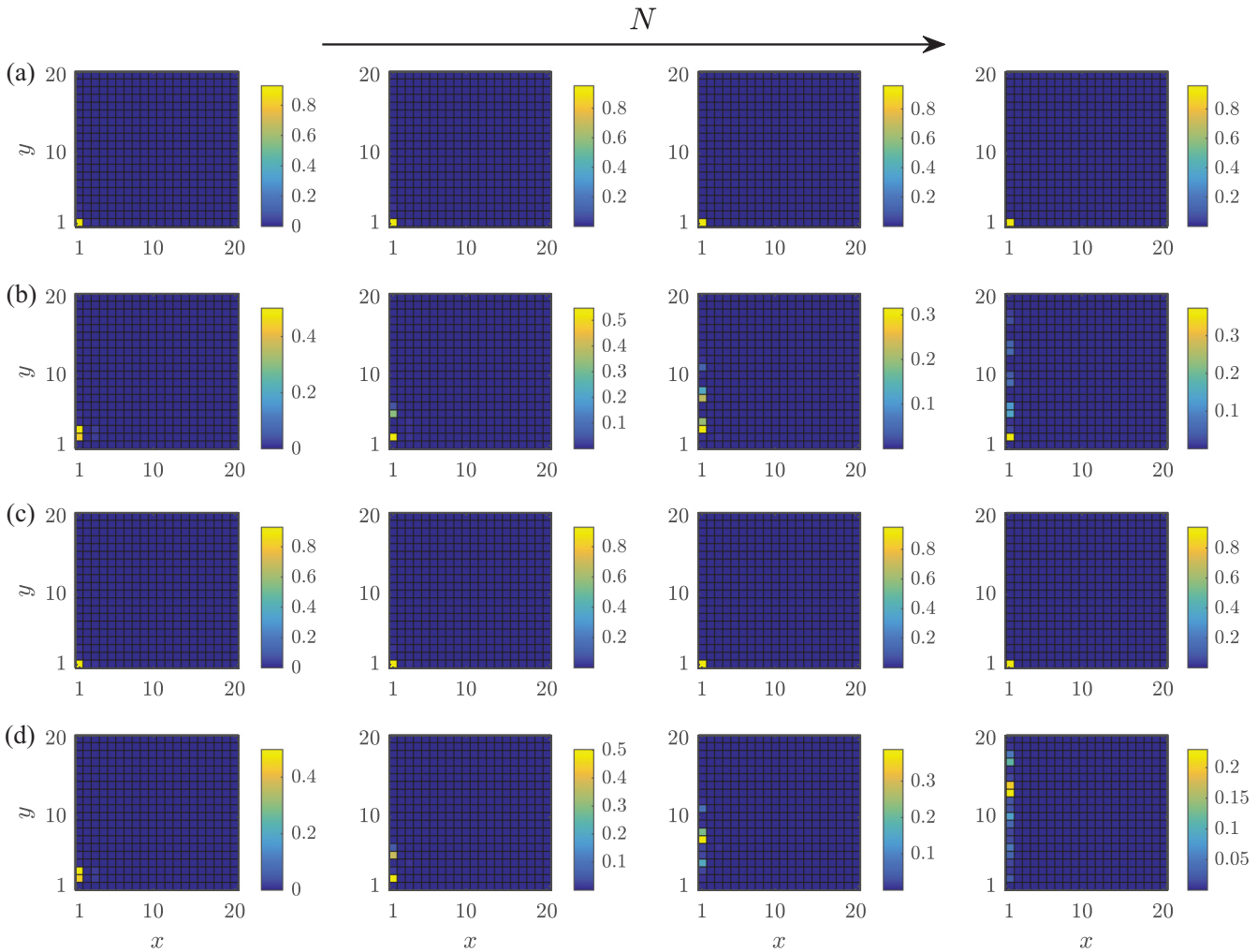

FIG. 7. The probability distributions of the coinless DTQWs on a 20×20 lattice for the static (a, b) and dynamic (c, d) disorders. The steps are chosen as $N = 5, 20, 50, 100$. The walker is initialized at one corner $(x, y) = (1, 1)$ (a, c) or edge $(x, y) = (1, 2)$ (b, d) of the lattice. The disorder strength $W/J_2 = 0.25$ and the parameter $J_1/J_2 = 0.1$. The results are obtained by averaging 100 independent disordered realizations.

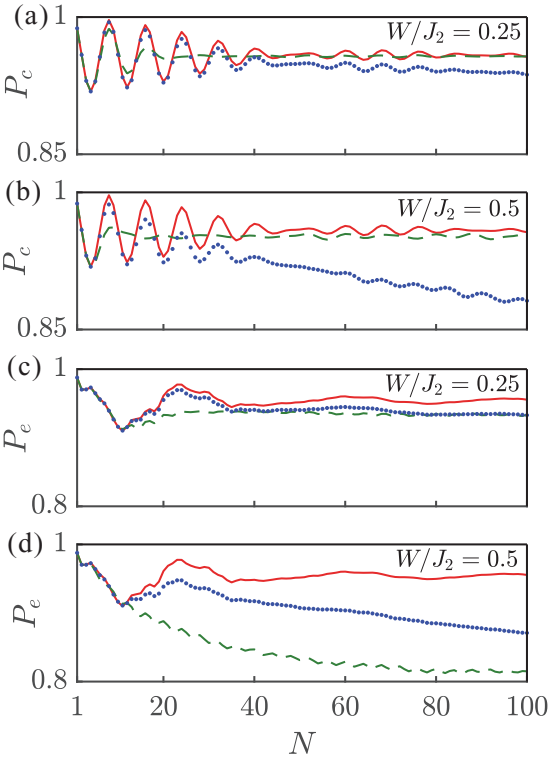

FIG. 8. (a, b) The probability P_c at the corner $(x, y) = (1, 1)$ vs the step N when the walker is initialized at the same corner. (c, d) The probability P_e at the left edge of the lattice vs step N when the walker is initialized at $(x, y) = (1, 2)$. The disorder strengths are chosen as $W/J_2 = 0.25$ (a, c) and $W/J_2 = 0.5$ (b, d). The dashed (dotted) lines represent the case with the static (dynamic) disorder. The solid lines represent the case without the disorder. The parameter $J_1/J_2 = 0.1$. The disordered results are obtained by averaging 100 independent disordered realizations.

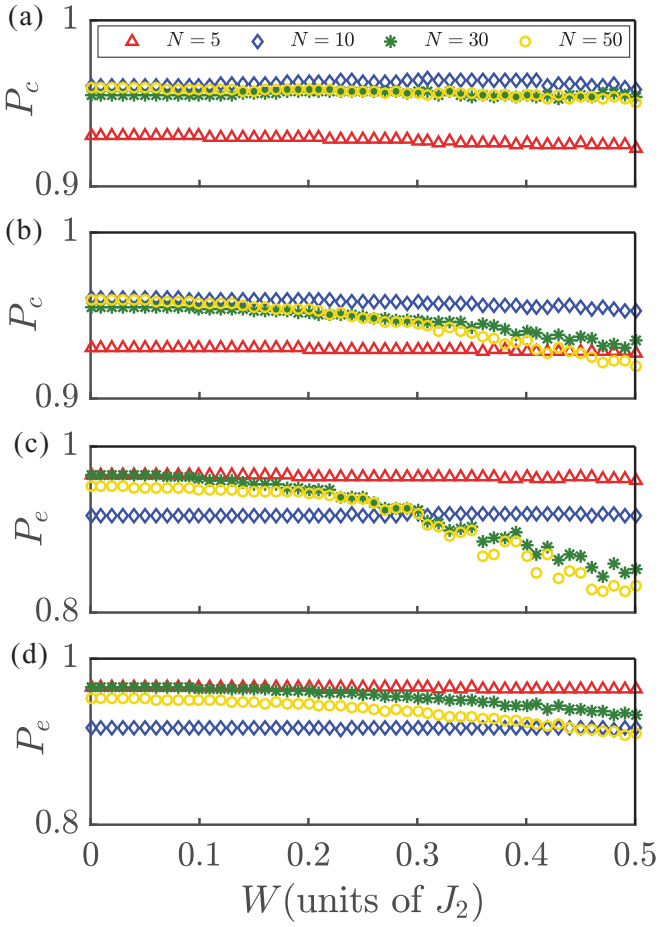

FIG. 9. (a, b) The probability P_c at the corner $(x, y) = (1, 1)$ vs the disorder strength W when the walker is initialized at the same corner. (c, d) The probability P_e at the left edge of the lattice vs the disorder strength W when the walker is initialized at $(x, y) = (1, 2)$. We consider the cases with the static (a, c) and dynamic (b, d) disorders. The steps are chosen as $N = 5, 10, 30, 50$ and the parameter $J_1/J_2 = 0.1$. The results are obtained by averaging 100 independent disordered realizations.

the step is small. When the step is large, the localizations at the corner and edge are still large but with slight decreases as we increase the disorder strength. Specifically, for the case with static disorder we can always observe nearly stable large localizations at the corner.

VII. CONCLUSIONS

In summary, we have constructed a two-dimensional coinless discrete-time quantum walk (DTQW) to simulate the second-order topological insulator. We have shown that both of the corner and edge states can be observed through the probability distribution independently. Finally, we have proposed a possible experimental implementation in a three-dimensional integrated photonic circuit and verified the robustness of the corner states against the small disorder. Since the coupling and phase between each of the two lattice sites at each step of the coinless DTQW can be adjusted independently, our scheme can be generalized directly to realize the non-Hermitian [59–64] and Floquet higher-order topological insulators [65–69]. Our work offers an alternative route to explore exotic higher-order topological matters using DTQWs.

ACKNOWLEDGMENTS

This work is supported partly by the National Key R&D Program of China under Grant No. 2017YFA0304203, the NSFC under Grant No. 11674200 and 1331KSC.

[1] Y. Aharonov, L. Davidovich, and N. Zagury, Quantum random walks, Phys. Rev. A **48**, 1687 (1993).

[2] E. Farhi and S. Gutmann, Quantum computation and decision trees, Phys. Rev. A **58**, 915 (1998).

[3] J. Kempe, Quantum random walks: An introductory overview, Contemp. Phys. **44**, 307 (2003).

[4] A. Patel, K. S. Raghunathan, and P. Rungta, Quantum random walks do not need a coin toss, Phys. Rev. A **71**, 032347 (2005).

[5] A. M. Childs, Universal Computation by Quantum Walk, Phys. Rev. Lett. **102**, 180501 (2009).

[6] A. M. Childs, D. Gosset, and Z. Webb, Universal computation by multiparticle quantum walk, Science **339**, 791 (2013).

[7] A. Aspuruguzik and P. Walther, Photonic quantum simulators, Nat. Phys. **8**, 285 (2012).

[8] F. Cardano, F. Massa, H. Qassim, E. Karimi, S. Slussarenko, D. Paparo, C. de Lisio, F. Sciarrino, E. Santamato, R. W. Boyd, and L. Marrucci, Quantum walks and wavepacket dynamics on a lattice with twisted photons, Sci. Adv. **1**, e1500087 (2015).

[9] O. Boada, L. Novo, F. Sciarrino, and Y. Omar, Quantum walks in synthetic gauge fields with three-dimensional integrated photonics, Phys. Rev. A **95**, 013830 (2017).

[10] F. Nejadsattari, Y. Zhanf, F. Bouchard, H. Larocque, A. Sit, E. Cohen, R. Fickler, and E. Karimi, Experimental realization of wave-packet dynamics in cyclic quantum walks, Optica **6**, 174 (2019).

[11] T. Kitagawa, M. S. Rudner, E. Berg, and E. Demler, Exploring topological phases with quantum walks, Phys. Rev. A **82**, 033429 (2010).

[12] J. K. Asbóth, Symmetries, topological phases, and bound states in the one-dimensional quantum walk, Phys. Rev. B **86**, 195414 (2012).

[13] J. K. Asbóth and H. Obuse, Bulk-boundary correspondence for chiral symmetric quantum walks, Phys. Rev. B **88**, 121406 (2013).

[14] H. Obuse, J. K. Asbóth, Y. Nishimura, and N. Kawakami, Unveiling hidden topological phases of a one-dimensional Hadamard quantum walk, Phys. Rev. B **92**, 045424 (2015).

[15] J. M. Edge and J. K. Asbóth, Localization, delocalization, and topological transitions in disordered two-dimensional quantum walks, Phys. Rev. B **91**, 104202 (2015).

[16] T. Rakovszky and J. K. Asbóth, Localization, delocalization, and topological phase transitions in the one-dimensional split-step quantum walk, Phys. Rev. A **92**, 052311 (2015).

[17] T. Groh, S. Brakhane, W. Alt, D. Meschede, J. K. Asbóth, and A. Alberti, Robustness of topologically protected edge states in quantum walk experiments with neutral atoms, Phys. Rev. A **94**, 013620 (2016).

[18] T. Rakovszky, J. K. Asbóth, and A. Alberti, Detecting topological invariants in chiral symmetric insulators via losses, Phys. Rev. B **95**, 201407 (2017).

[19] V. V. Ramasesh, E. Flurin, M. Rudner, I. Siddiqi, and N. Y. Yao, Direct Probe of Topological Invariants using Bloch Oscillating Quantum Walks, Phys. Rev. Lett. **118**, 130501 (2017).

[20] M. Sajid, J. K. Asbóth, D. Meschede, R. F. Werner, and A. Alberti, Creating anomalous Floquet Chern insulators with magnetic quantum walks, Phys. Rev. B **99**, 214303 (2019).

[21] T. Kitagawa, M. A. Broome, A. Fedrizzi, M. S. Rudner, E. Berg, I. Kassal, A. Aspuru-Guzik, E. Demler, and A. G. White, Observation of topologically protected bound states in photonic quantum walks, Nat. Commun. **3**, 882 (2012).

[22] F. Cardano, M. Maffei, F. Massa, B. Piccirillo, C. de Lisio, G. De Filippis, V. Cataudella, E. Santamato, and L. Marrucci, Statistical moments of quantum-walk dynamicas reveal topological quantum transitions, Nat. Commun. **7**, 11439 (2016).

[23] F. Cardano, A. D'Errico, A. Dauphin, M. Maffei, B. Piccirillo, C. D. Lisio, G. D. Filippis, V. Cataudella, E. Santamato, L. Marrucci, M. Lewenstein, and P. Massignan, Detection of Zak phases and topological invariants in a chiral quantum walk of twisted photons, Nat. Commun. **8**, 15516 (2017).

[24] E. Flurin, V. V. Ramasesh, S. Hacohen-Gourgy, L. S. Martin, N. Y. Yao, and I. Siddiqi, Observing Topological Invariants Using Quantum Walks in Superconducting Circuits, Phys. Rev. X **7**, 031023 (2017).

[25] X.-Y. Xu, Q.-Q. Wang, W.-W. Pan, K. Sun, J.-S Xu, G. Chen, J.-S. Tang, M. Gong, Y.-J. Han, C.-F. Li, and G.-C. Guo, Measuring the Winding Number in a Large-Scale Chiral Quantum Walk, Phys. Rev. Lett. **120**, 260501 (2018).

[26] D.-Z. Xie, T.-S. Deng, T. Xiao, W. Gou, T. Chen, W. Yi, and B. Yan, Topological Quantum Walks in Momentum Space with a Bose-Einstein Condensate, Phys. Rev. Lett. **124**, 050502 (2020).

[27] L. Xiao, X. Zhan, Z.-H. Bian, K.-K. Wang, X. Zhang, X.-P. Wang, J. Li, K. Mochizuki, D. Kim, N. Kawakami, W. Yi, H. Obuse, B. C. Sanders, and P. Xue, Observation of topological edge states in parity-time-symmetric quantum walks, Nat. Phys. **13**, 1117 (2017).

[28] X. Zhan, L. Xiao, Z.-H. Bian, K.-K. Wang, X.-Z. Qiu, B. C. Sanders, W. Yi, and P. Xue, Detecting Topological Invariants in Nonunitary Discrete-Time Quantum Walks, Phys. Rev. Lett. **119**, 130501 (2017).

[29] K.-K. Wang, X.-Z. Qiu, L. Xiao, X. Zhan, Z.-H. Bian, B. C. Sanders, W. Yi, and P. Xue, Observation of emergent momentum-time skyrmions in parity-time-symmetric non-unitary quench dynamics, Nat. Commun. **10**, 2293 (2019).

[30] K.-K. Wang, X.-Z. Qiu, L. Xiao, X. Zhan, Z.-H. Bian, W. Yi, and P. Xue, Simulating Dynamic Quantum Phase Transitions in Photonic Quantum Walks, Phys. Rev. Lett. **122**, 020501 (2019).

[31] L. Xiao, K.-K. Wang, X. Zhan, Z.-H. Bian, K. Kawabata, M. Ueda, W. Yi, and P. Xue, Observation of Critical Phenomena in Parity-Time-Symmetric Quantum Dynamics, Phys. Rev. Lett. **123**, 230401 (2019).

[32] B. Wang, T. Chen, and X. Zhang, Experimental Observation of Topologically Protected Bound States with Vanishing Chern Numbers in a Two-Dimensional Quantum Walk, Phys. Rev. Lett. **121**, 100501 (2018).

[33] C. Chen, X. Ding, J. Qin, Y. He, Y. Luo, M. Chen, C. Liu, X. Wang, W. Zhang, H. Li, L. You, Z. Wang, D. Wang, B. C. Sanders, C. Lu, and J. Pan, Observation of Topologically Protected Edge States in a Photonic Two-Dimensional Quantum Walk, Phys. Rev. Lett. **121**, 100502 (2018).

[34] H. Chalabi, S. Barik, S. Mittal, T. E. Murphy, M. Hafezi, and E. Waks, Synthetic Gauge Field for Two-Dimensional Time-Multiplexed Quantum Random Walks, Phys. Rev. Lett. **123**, 150503 (2019).

[35] A. D'Errico, F. Cardano, M. Maffei, A. Dauphin, R. Barboza, C. Esposito, B. Piccirillo, M. Lewenstein, P. Massignan, and L. Marrucci, Two-dimensional topological quantum walks in the momentum space of structured light, Optica **7**, 108 (2020).

[36] R. Portugal, S. Boettcher, and S. Falkner, One-dimensional coinless quantum walks, Phys. Rev. A **91**, 052319 (2015).

[37] R. A. M. Santos, R. Portugal, and S. Boettcher, Moments of coinless quantum walks on lattices, Quant. Inf. Process. **14**, 3179 (2015).

[38] R. Portugal, M. C. de Oliveira, and J. K. Moqadam, Staggered quantum walks with Hamiltonians, Phys. Rev. A **95**, 012328 (2017).

[39] J. K. Moqadam, M. C. de Oliveira, and R. Portugal, Staggered quantum walks with superconducting microwave resonators, Phys. Rev. B **95**, 144506 (2017).

[40] B. Chagas and R. Portugal, Discrete-time quantum walks on oriented graphs, EPTCS **315**, 26 (2020).

[41] R. Portugal, Quantum Walks and Search Algorithms (Springer, New York, 2013).

[42] R. Portugal and T. D. Fernandes, Quantum search on the two-dimensional lattice using the staggered model with Hamiltonians, Phys. Rev. A **95**, 042341 (2017).

[43] J. K. Moqadam and A. T. Rezakhani, Boundary-induced coherence in the staggered quantum walk on different topologies, Phys. Rev. A **98**, 012123 (2018).

[44] W. A. Benalcazar, B. A. Bernevig, and T. L. Hughes, Quantized electric multipole insulators, Science **357**, 61 (2017).

[45] W. A. Benalcazar, B. A. Bernevig, and T. L. Hughes, Electric multiple moments, topological multipolemoment pumping, and chiral hinge states in crystalline insulators, Phys. Rev. B **96**, 245115 (2017).

[46] J. Langbehn, Y. Peng, L. Trifunovic, F. von Oppen, and P. W. Brouwer, Reflection-Symmetric Second-Order Topological Insulators and Superconductors, Phys. Rev. Lett. **119**, 246401 (2017).

[47] Z. Song, Z. Fang, and C. Fang, (d-2)-Dimensional Edge States of Rotation Symmetry Protected Topological States, Phys. Rev. Lett. **119**, 246402 (2017).

[48] F. Schindler, A. M. Cook, M. G. Vergniory, Z. Wang, S. S. P. Parkin, B. A. Bernevig, and T. Neupert, Higher-order topological insulators, Sci. Adv. **4**, eaat0346 (2018).

[49] M. Serra-Garcia, V. Peri, R. Süsstrunk, O. R. Bilal, T. Larsen, L. G. Villanueva, and S. D. Huber, Observation of a phononic quadrupole topological insulator, Nature (London) **555**, 342 (2018).

[50] C. W. Peterson, W. A. Benalcazar, T. L. Hughes, and G. Bahl, A quantized microwave quadrupole insulator with topologically protected corner states, Nature (London) **555**, 346 (2018).

[51] F. Schindler, Z.-J. Wang, M. G. Vergniory, A. M. Cook, A. Murani, S. Sengupta, A. Y. Kasumov, R. Deblock, S. Jeon, I. Drozdov, H. Bouchiat, S. Guéron, A. Yazdani, B. A. Bernevig, and T. Neupert, Higher-order topology in bismuth, Nat. Phys. **14**, 918 (2018).

[52] S. Imhof, C. Berger, F. Bayer, J. Brehm, L. Molenkamp, T. Kiessling, F. Schindler, C. H. Lee, M. Greiter, T. Neupert, and R. Thomale, Topological-circuit realization of topological corner modes, Nat. Phys. **14**, 925 (2018).

[53] S. Mittal, V. V. Orre, G. Zhu, M. A. Gorlach, A. Poddubny, and M. Hafezi, Photonic quadrupole topological phases, Nat. Photon. **13**, 692 (2019).

[54] H.-R. Xue, Y.-H. Yang, F. Gao, Y.-D. Chong, and B.-L. Zhang, Acoustic higher-order topological insulator on a kagome lattice, Nat. Mater. **18**, 108 (2019).

[55] A. E. Hassan, F. K. Kunst, A. Moritz, G. Andler, E. J. Bergholtz, and M. Bourennane, Corner states of light in photonic waveguides, Nat. Photon. **13**, 697 (2019).

[56] F. Zangeneh-Nejad and R. Fleury, Nonlinear Second-Order Topological Insulators, Phys. Rev. Lett. **123**, 053902 (2019).

[57] Y. You, D. Litinski, and F. von Oppen, Higher-order topological superconductors as generators of quantum codes, Phys. Rev. B **100**, 054513 (2019).

[58] K. Laubscher, D. Loss, and J. Klinovaja, Fractional topological superconductivity and parafermion corner states, Phys. Rev. Res. **1**, 032017 (2019).

[59] C. H. Lee, L. Li, and J. Gong, Hybrid Higher-Order Skin-Topological Modes in Nonreciprocal Systems, Phys. Rev. Lett. **123**, 016805 (2019).

[60] T. Liu, Y.-R. Zhang, Q. Ai, Z. Gong, K. Kawabata, M. Ueda, and F. Nori, Second-Order Topological Phases in Non-Hermitian Systems, Phys. Rev. Lett. **122**, 076801 (2019).

[61] X.-W. Luo and C.-W. Zhang, Higher-Order Topological Corner States Induced by Gain and Loss, Phys. Rev. Lett. **123**, 073601 (2019).

[62] E. Edvardsson, F. K. Kunst, and E. J. Bergholtz, Non-Hermitian extensions of higher-order topological phases and their biorthogonal bulk-boundary correspondence, Phys. Rev. B **99**, 081302 (2019).

[63] M. Ezawa, Non-Hermitian boundary and interface states in nonreciprocal higher-order topological metals and electrical circuits, Phys. Rev. B **99**, 121411 (2019).

[64] M. Ezawa, Non-Hermitian higher-order topological states in nonreciprocal and reciprocal systems with their electric-circuit realization, Phys. Rev. B **99**, 201411 (2019).

[65] M. Rodriguez-Vega, A. Kumar, and B. Seradjeh, Higher-order Floquet topological phases with corner and bulk bound states, Phys. Rev. B **100**, 085138 (2019).

[66] R. W. Bomantara, L. Zhou, J. Pan, and J. Gong, Coupled-wire construction of static and Floquet second-order topological insulators, Phys. Rev. B **99**, 045441 (2019).

[67] R. Seshadri, A. Dutta, and D. Sen, Generating a second-order topological insulator with multiple corner states by periodic driving, Phys. Rev. B **100**, 115403 (2019).

[68] Y. Peng and G. Refael, Floquet Second-Order Topological Insulators from Nonsymmorphic Space-Time Symmetries, Phys. Rev. Lett. **123**, 016806 (2019).

[69] H. Hu, B. Huang, E. Zhao, and W. Vincent Liu, Dynamical Singularities of Floquet Higher-Order Topological Insulators, Phys. Rev. Lett. **124**, 057001 (2020).

[70] S. Gross and M. J. Withford, Ultrafast-laser-inscribed 3D integrated photonics: Challenges and emerging applications, Nanophotonics **4**, 332 (2015).

[71] L. Sansoni, F. Sciarrino, G. Vallone, P. Mataloni, A. Crespi, R. Ramponi, and R. Osellame, Two-Particle Bosonic-Fermionic Quantum Walk via Integrated Photonics, Phys. Rev. Lett. **108**, 010502 (2012).

[72] K. Okamoto, *Fundamentals and Applications of Optical Waveguides* (Elsevier, San Diego, CA, 2006).

[73] A. Crespi, R. Osellame, R. Ramponi, V. Giovannetti, R. Fazio, L. Sansoni, F. D. Nicola, F. Sciarrino, and P. Mataloni, Anderson localization of entangled photons in an integrated quantum walk, Nat. Photon. **7**, 322 (2013).

[74] A. Crespi, R. Osellame, R. Ramponi, D. J. Brod, E. F. Galvão, N. Spagnolo, C. Vitelli, E. Maiorino, P. Mataloni, and F. Sciarrino, Integrated multimode interferometers with arbitrary designs for photonic boson sampling, Nat. Photon. **7**, 545 (2013).

[75] S. Nolte, M. Will, J. Burghoff, and A. Tuennermann, Femtosecond waveguide writing: A new avenue to three-dimensional integrated optics, Appl. Phys. A **77**, 109 (2003).

[76] N. Spagnolo, C. Vitelli, L. Sansoni, E. Maiorino, P. Mataloni, F. Sciarrino, D. J. Brod, E. F. Galvaõ, A. Crespi, R. Ramponi, and R. Osellame, General Rules for Bosonic Bunching In multimode Interferometers, Phys. Rev. Lett. **111**, 130503 (2013).

[77] H. Tang, X.-F. Lin, Z. Feng, J.-Y. Chen, J. Gao, K. Sun, C.-Y. Wang, P.-C. Lai, X.-Y. Xu, Y. Wang, L.-F. Qiao, A.-L. Yang, and X.-M. Jin, Experimental two-dimensional quantum walk on a photonic chip, Sci. Adv. **4**, eaat3174 (2018).

[78] H. Tang, C. D. Franco, Z.-Y. Shi, T.-S. He, Z. Feng, J. Gao, K. Sun, Z.-M. Li, Z.-Q. Jiao, T.-Y. Wang, M. S. Kim, and X.-M. Jin, Experimental quantum fast hitting on hexagonal graphs, Nat. Photon. **12**, 754 (2018).